CHEMISTRY OF MATERIALS
Article

Chem. Mater. **2009,** *21,* 4071–4079 4071
DOI:10.1021/cm901560e

Thermoresponsive Dual-Phase Transition and 3D Self-Assembly of Poly(*N*-Isopropylacrylamide) Tethered to Silicate Platelets

Yu-Min Chen,[†] Hsiao-Chu Lin,[†] Ru-Siou Hsu,[†] Bi-Zen Hsieh,[†] Yu-An Su,[†] Yu-Jane Sheng,*[,†,‡] and Jiang-Jen Lin*[,†]

[†]*Institute of Polymer Science and Engineering, and* [‡]*Department of Chemical Engineering, National Taiwan University, Taipei 10617, Taiwan*

Received June 6, 2009. Revised Manuscript Received July 28, 2009

Thermoresponsive poly(*N*-isopropylacrylamide) (PNiPAAm) was covalently tethered to nanosilicate platelets (NSP) to generate a new class of organic−inorganic hybrid that exhibits self-assembly and phase transformation properties under applied stimuli. Hybrids of two grafting densities were prepared and the PNiPAAm length was precisely controlled to yield a degree of polymerization of 350−1890 and a narrow molecular weight distribution (1.21−1.50 polydispersity or M_w/M_n). Two distinctive second-order transitions were observed during differential scanning calorimetry analysis, indicating the existence of dual-segment density zones. The difference between the two transition temperatures gradually vanished with increasing chain length, and a single endothermic first-order transition emerged. The hybrid also underwent a heat-induced phase transformation after treatment with several heating and cooling cycles. It is believed that fixation of PNiPAAm onto NSP greatly inhibited chain relaxation movements and hindered reversible coil−globule transitions. Furthermore, thermally induced self-assembly behavior was directly observed by transmission electronic microscopy of the hybrid coating as a thin film on a silicon wafer surface. The formation of a 3D network of nanostructures was directed by the platelet shape at temperatures higher than the critical solution temperature of the PNiPAAm chains. The temperature-controllable phase separation for formation of an ordered domain network of 100−500 nm in dimension has potential for the fabrication of new smart nanomaterials.

Introduction

Over the past decade, poly(*N*-isopropylacrylamide) (PNiPAAm) has received a great deal of attention as a thermoresponsive polymer. The polymer exhibits lower critical solution temperature (LCST) behavior at 32 °C and undergoes a coil-to-globule phase transition induced by expulsion of water from the chain.[1] Stimulus-responsive polymers have been widely reported for hybrid forms attached to nanoparticles or solid substrates including wafers,[2] SiO_2,[3,4] Au,[5,6] carbon nanotubes,[7] Fe_3O_4,[8] and layered silicates[9] for use as materials that respond to external triggers. Potential applications of such smart behavior include sensors,[10] probes,[11] drug delivery,[12] and biomaterial separation.[13]

Two-dimensional layered silicates have a platelike geometric shape of nanometer thickness and a high aspect ratio. Naturally occurring smectite clays are conventionally used as catalysts,[14] absorbents,[15] and polymer/clay nanocomposites.[16,17] The clays are generally hydrophilic in nature and require organic modification using ionic exchange agents such as alkylammonium derivatives[18] or phosphonium salts.[19] Organic incorporation into the interlayer gallery renders the clay compatible with a hydrophobic polymer matrix and is suitable for improving the properties of nanocomposites.[20] In contrast to the hydrophobic properties, hydrophilic silicates are suitable

*Corresponding author. E-mail: jianglin@ntu.edu.tw (J. J. Lin); E-mail: yjsheng@ntu.edu.tw (Y. J. Sheng).

(1) Shibayama, M.; Suetoh, Y.; Nomura, S. *Macromolecules* **1996**, *29*, 6966.
(2) Luzinov, I.; Minko, S.; Tsukruk, V. V. *Prog. Polym. Sci.* **2004**, *29*, 635.
(3) (a) von Werne, T.; Patten, T. E. *J. Am. Chem. Soc.* **1999**, *121*, 7409. (b) von Werne, T.; Patten, T. E. *J. Am. Chem. Soc.* **2001**, *123*, 7497.
(4) Schepelina, O.; Zharov, I. *Langmuir* **2008**, *24*, 14188.
(5) Yusa, S.; Fukuda, K.; Yamamoto, T.; Iwasaki, Y.; Watanabe, A.; Akiyoshi, K.; Morishima, Y. *Langmuir* **2007**, *23*, 12842.
(6) Kaholek, M.; Lee, W. K.; Ahn, S. J.; Ma, H.; Caster, K. C.; LaMattina, B.; Zauscher, S. *Chem. Mater.* **2004**, *16*, 3688.
(7) Kong, H.; Li, W.; Gao, C.; Yan, D.; Jin, Y.; Walton, D. R. M.; Kroto, H. W. *Macromolecules* **2004**, *37*, 6683.
(8) Lattuada, M.; Hatton, T. A. *Langmuir* **2007**, *23*, 2158.
(9) Yang, Y.; Liu, L.; Zhang, J.; Li, C.; Zhao, H. *Langmuir* **2007**, *23*, 2867.
(10) Wang, X.; Kim, Y. G.; Drew, C.; Ku, B. C.; Kumar, J.; Samuelson, L. A. *Nano Lett.* **2004**, *4*, 331.
(11) De, M.; Ghosh, P. S.; Rotello, V. M. *Adv. Mater.* **2008**, *20*, 1.
(12) Soppinmath, K. S.; Tan, D. C. W.; Yang, Y. Y. *Adv. Mater.* **2005**, *17*, 318.
(13) Rzayev, J.; Hillmyer, M. A. *J. Am. Chem. Soc.* **2005**, *127*, 13373.
(14) Pinnavaia, T. J. *Science* **1983**, *220*, 365.
(15) Theng, B. K. G. *The Chemistry of Clay-Organic Reactions*; John Wiley & Sons: New York, 1974.
(16) Giannelis, E. P. *Adv. Mater.* **1996**, *8*, 29.
(17) Ray, S. S.; Okamoto, M. *Prog. Polym. Sci.* **2003**, *28*, 1539.
(18) (a) Lin, J. J.; Cheng, I. J.; Wang, R.; Lee, R. J. *Macromolecules* **2001**, *34*, 8832. (b) Lin, J. J.; Chen, Y. M. *Langmuir* **2004**, *20*, 4261.
(19) Ijdo, W. L.; Pinnavaia, T. J. *Chem. Mater.* **1999**, *11*, 3227.
(20) Xu, R.; Manias, E.; Snyder, A. J.; Runt, J. *Macromolecules* **2001**, *34*, 337.

Published on Web 08/10/2009

for mixing with water-soluble polymers such as PNiPAAm to be made of nanocomposite gels (NC hydrogels).[21a] The NC gels have different mechanical,[21b] optical,[21c] and thermal response properties[21d] than the conventional hydrogels by organic cross-linking agents.

Manipulated architectures of polymeric brushes grafted from layered silicates was reported, including the synthesis of an azo-containing compound by free radical polymerization[22] and living polymerization methodologies that include anionic living polymerization,[23] nitroxide-mediated polymerization,[24] reversible addition−fragmentation chain transfer,[25] and atom transfer radical polymerization (ATRP).[26] These approaches generally involve ionic bonding between the polymers and silicates through ionic exchange reaction of the initiator into the clay gallery and subsequent polymerization. However, little work has focused on growing polymer brushes by covalent bonding to plate-shaped silicates, perhaps because of geometric hindrance and because silanol (≡Si−OH) groups exist only on the edge of the clay sheets in the natural layered structure.[27] In our previous studies, oligomeric amines consisting of hydrophobic poly(oxypropylene) segments and multiple amine functionalities were used to exfoliate hydrophilic clays. The original layered clay structure is randomized into individual silicate plates. A subsequent extraction process allows isolation of the exfoliated nanosilicate platelets (NSP) in aqueous suspension. The plate material has average dimensions of 80 nm × 80 nm × 1 nm and a charge distribution of 2×10^4 ionic charges in each plate. These isolated sheetlike silicate materials are different from pristine layered silicates with respect to their ionic charge exposure[28a] and dispersing or self-assembling behavior.[28b]

In the present study, we used a living polymerization technique to graft moieties to the NSP edge surface through covalent bonding to produce polymer. This tethering of thermoresponsive polymer strain to silicate plates via covalent bonding has not yet been reported in the literature. A novel linker with a dual active site was synthesized and first covalently attached to NSP. Subsequent ATRP was carried out to grow the PNiPAAm strain. NSP-PNiPAAm of well-defined chain length and different graft densities exhibited two specific phase transitions. This unique behavior was investigated using differential scanning calorimetry (DSC). The formation of 3D nanostructures via thermally tailored self-assembly behavior was observed by transmission electronic microscopy (TEM).

Experimental Section

Materials. Copper(I) chloride (CuCl, 95%, Acros) was successively washed with glacial acetic acid (Fisher Scientific) and ethanol and then dried under a vacuum. 2-Hydroxyethyl acrylate (HEA; 97%, Acros) was distilled before use. 2-Bromo-2-methylpropionyl bromide (98%, Acros), 3-aminopropyltriethoxylsilane (APTES, TCI) and *N*,*N*,*N*′,*N*″,*N*″′-pentamethyldiethylenetriamine (PMDETA, 99%, TCI) were used as received. *N*-Isopropylacrylamide (NiPAAm, 99%, Acros) was purified by recrystallization from *n*-hexane and dried under a vacuum. Sodium montmorillonite (Na^+-MMT), a sodium form of smectite aluminosilicate, was obtained from Nanocor Co. These naturally occurring clays have a 2:1 layered silicate/aluminum oxide structure in which two tetrahedral sheets sandwich an edge-shared octahedral sheet. The commercially available clay has exchangeable Na^+ counterions with a cationic exchange capacity of 120 mequiv/100 g and an average of 8−10 sheets in a primary stack. The size of individual platelets in the polydisperse MMT primary stack is estimated to be 80−100 nm in width and 1 nm in thickness.[18] Individual silicate platelets were obtained by delaminating the layered mineral using an exfoliation process developed by our research group[29] and subsequent extraction with sodium hydroxide.

Synthesis of the Bis-bromo-triethoxysilane (BBTES) Linker with Bromide and Triethoxysilane Functionalities. HEA (5.0 g, 0.043 mol) and triethylamine (4.3 g, 0.043 mol) in anhydrous tetrahydrofuran (THF; 30 mL) were added to a three-necked round-bottomed flask equipped with a magnetic stirrer and nitrogen inlet−outlet lines. 2-Bromo-2-methylpropionyl bromide (9.9 g, 0.043 mol) dissolved in THF (10 mL) was slowly added dropwise with stirring at 4 °C under nitrogen. The mixture was stirred for 3 h and then heated to room temperature (rt) and stirred for 12 h. During the process, the hydrochloric acid/amine salt appeared as a white precipitate. The mixture was then filtered through filter paper (Whatman No. 5) using a Buchner Funnel attached to an aspirator. The filtrate was concentrated in a rotary evaporator at 30 °C under reduced pressure. The bromo-terminated acrylate product was recovered in nearly quantitative yield. The product was dissolved in THF (50 mL) and placed in a round-bottom flask sealed with a rubber septum and purged with nitrogen for 30 min. APTES (6.2 g, 0.028 mmol) was added to the mixture and agitated at 50 °C for 12 h. The solvent was then removed using a rotary evaporator. The resulting solution was poured into a large excess of hexane and settled into two phases. Excess amounts of APTES and the unfavorable monosubstituted analogue could be removed by the hexane phase. The resulting product (BBTES) was dried under vacuum to give a transparent light yellow viscous material (15.2 g, 72% yield). ^{1}H NMR spectroscopic analysis revealed the following results ($CDCl_3$, δ, in ppm, 400 MHz): 4.35−4.31 [8H; $-N(CH_2CH_2COOCH_2CH_2OCOC(CH_3)_2Br)_2$], 3.70−3.73 [6H; $(CH_3CH_2O)_3Si-$], 2.73 [4H; $-N(CH_2CH_2COOCH_2CH_2OCOC(CH_3)_2Br)_2$], 2.33 [2H; $(CH_3CH_2)_3SiCH_2-$

(21) (a) Haraguchi, K.; Takehisa, T.; Fan, S. *Macromolecules* **2002**, *35*, 10162. (b) Haraguchi, K.; Takehisa, T. *Adv. Mater.* **2002**, *14*, 1120. (c) Murata, K; Haraguchi, K. *J. Mater. Chem.* **2007**, *17*, 3385. (d) Liang, L.; Liu, J.; Gong, X. *Langmuir* **2000**, *16*, 9895.
(22) Fan, X.; Xia, C.; Advincula, R. C. *Langmuir* **2003**, *19*, 4381.
(23) Zhou, Q.; Fan, X.; Xia, C.; Mays, J.; Advincula, R. *Chem. Mater.* **2001**, *13*, 2465.
(24) (a) Weimer, M. W.; Giannelis, E. P.; Sogah, D. Y. *J. Am. Chem. Soc.* **1999**, *121*, 1615. (b) Di, J.; Sogah, D. Y. *Macromolecules* **2006**, *39*, 5052.
(25) (a) Shah, D.; Fytas, G.; Vlassopoulos, D.; Di, J.; Sogah, D. Y.; Giannelis, E. P. *Langmuir* **2005**, *21*, 19. (b) Di, J.; Sogah, D. Y. *Macromolecules* **2006**, *39*, 1020.
(26) (a) Zhao, H.; Shipp, D. A. *Chem. Mater.* **2003**, *15*, 2693. (b) Sedjo, R. A.; Mirous, B. K.; Brittain, W. J. *Macromolecules* **2000**, *33*, 1492.
(27) (a) Wheeler, P. A.; Wang, J.; Baker, J.; Mathias, L. J. *Chem. Mater.* **2005**, *17*, 3012. (b) Wheeler, P. A.; Wang, J.; Mathias, L. J. *Chem. Mater.* **2006**, *18*, 3937.
(28) (a) Lin, J. J.; Chu, C. C.; Chiang, M. L.; Tsai, W. C. *J. Phys. Chem. B* **2006**, *110*, 18115. (b) Lin, J. J.; Chu, C. C.; Chou, C. C.; Shieu, F. S. *Adv. Mater.* **2005**, *17*, 301.
(29) Chu, C. C.; Chiang, M. L.; Tsai, C. M.; Lin, J. J. *Macromolecules* **2005**, *38*, 6240.

Scheme 1. (A) Synthesis of the Linker by Esterification and Michael Addition; (B) Tethering onto NSP Edges by Sol−Gel Reaction; (C) Conceptual Diagram of NSP-PNiPAAm formation by the ATRP "Grafting From" Method and Morphological Transformation at LCST

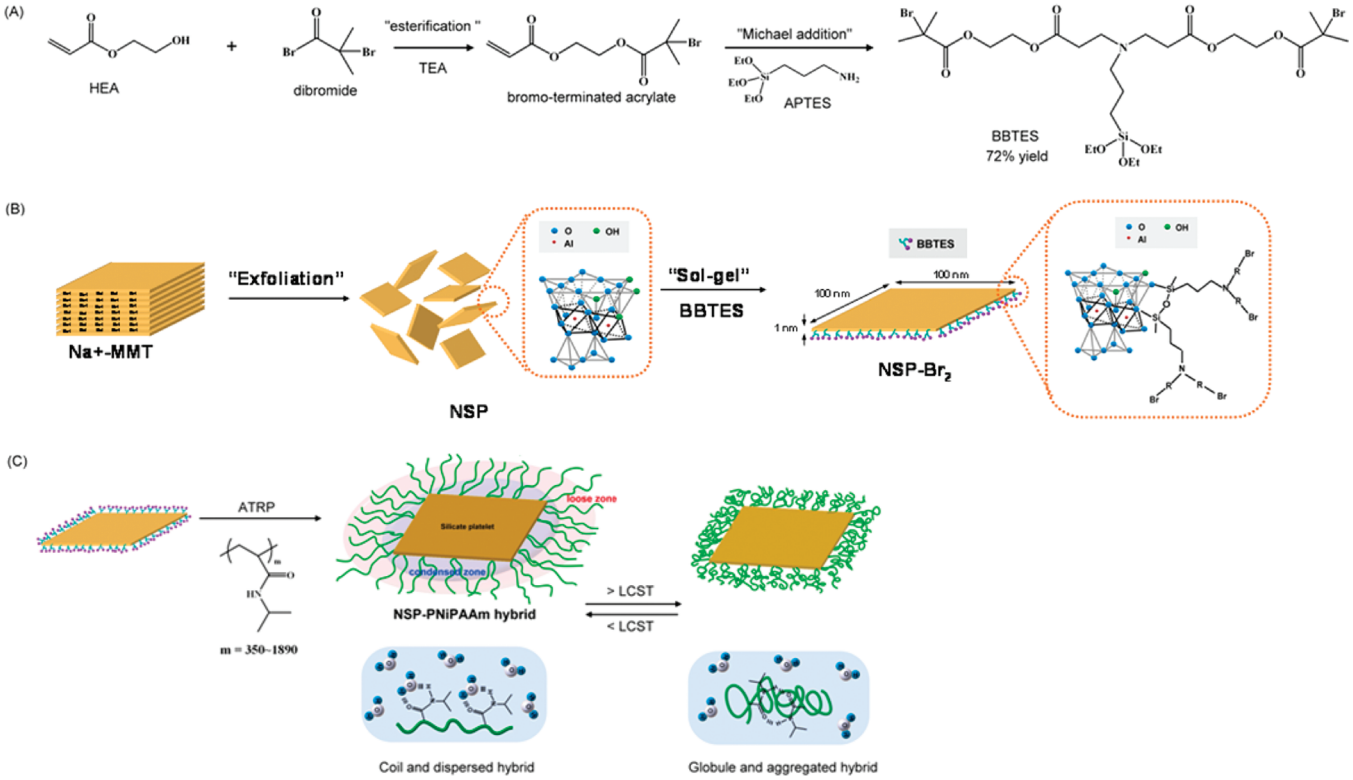

CH_2CH_2N-], 1.91−1.81 [12H; $-N(CH_2CH_2COOCH_2CH_2OCOC(CH_3)_2Br)_2$], 1.20 [9H; $(CH_3CH_2O)_3Si-$], 1.43 [2H; $(CH_3CH_2)_3SiCH_2CH_2CH_2-$], 0.56 [2H; $(CH_3CH_2O)_3SiCH_2CH_2CH_2-$].

Preparation of NSP-Br_2. The grafting density was varied by adding different amounts of BBTES to NSP. In a typical procedure, NSP (2 g) and THF (100 mL) were added to a 250 mL round-bottom flask sealed with a rubber septum and the slurry was stirred until the NSP was well dispersed. BBTES (0.4 g) in THF (5 mL) was added to NSP slurry prepared separately in THF (5 mL) to give a BBTES/NSP weight ratio of 5:1. The slurry was stirred at 50 °C for 2 days and the product was then collected by centrifugation at 2000 rpm and redispersed by stirring in methanol (100 mL) for 1 h. After three washing cycles, the product (NSP-Br_2) was dried at 50 °C for 24 h under reduced pressure before thermogravimetric analysis (TGA). The amount of organic material grafted was calculated as follows

$$\text{grafted amount (mequiv/g)} = \frac{10^3 \times (W_{250-600}) \times 2}{M} \qquad (1)$$

where M is the molecular weight of BBTES (588 g/mol) and $W_{250-600}$ is the weight loss per gram of the hybrid between 250 and 600 °C during TGA.

ATRP Gafting of PNiPAAm. NSP-PNiPAAm or NSP-polymer hybrids were prepared by ATRP using CuCl/PMDETA as the catalyst. In a typical procedure, NSP-Br_2 (0.5 g, 0.09 mmol), NiPAAm (2.9 g, 25.7 mmol), and MeOH/H_2O (7/3 vol.%, 15 mL) were individually added to a 50 mL Schlenk flask, degassed by three freeze−pump−thaw cycles, and kept under nitrogen. PMDETA (0.015 g, 0.08 mmol), CuCl (0.008 g, 0.08 mmol), and MeOH/H_2O (7/3 vol.%, 5 mL) were individually added to a 10 mL Schlenk flask, and the solution was degassed using three freeze−pump−thaw cycles. The formation of the Cu/ligand complex was observed as a solution color change from colorless to light blue. After catalyst formation, the solution was transferred by syringe to the Schlenk flask containing the NSP-Br_2/NiPAAm mixture under nitrogen. The solution was stirred at rt for 24 h to allow polymerization to proceed. The product, NSP-PNiPAAm, was isolated by centrifugation, washed at least three times with deionized water, and dried at 50 °C in a vacuum oven. The isolated product appeared to be blue colored because of the contamination of Cu/ligand catalyst. The same phenomena was also observed in the hydrated Na−clay system.[30]

Characterization. ^1H NMR spectra (in $CDCl_3$ with tetramethylsilane as the standard reference) were recorded on a Bruker AMX400 instrument operating at 400 MHz. Solid-state ^{29}Si NMR experiments were carried out at 59.6 MHz on a Bruker DSX300 NMR spectrometer equipped with a commercial 7-mm magic-angle spinning (MAS) NMR probe with an MAS frequency of 5 kHz (tetramethylsilane as the external reference). The molecular weight was estimated by gel permeation chromatography (GPC) performed on a Waters system (model 515 HPLC pump, model 717 autosampler, and model 2410 refractive index detector). A Waters Styragel column set, eluted with THF at 1.0 mL/min, was used to determine the relative molecular weight calibrated against polystyrene standards. Fourier-transform infrared (FT-IR) spectra were recorded on a Perkin-Elmer Spectrum One FT-IR spectrometer over the range 400−4000 cm^{-1}. The organic content was analyzed by TGA on a Perkin-Elmer Pyris 1 instrument. The temperature was increased from 100 to 900 at 10 °C/min in air. Dissolution in water (0.1 wt %) as a function of temperature was determined by measuring the transmittance on a UV−visible spectrophotometer (Shimadzu UV mini 1240) at 550 nm. The

(30) Munirasu, S.; Deshpande, A.; Baskaran, D. *Macromol. Rapid Commun.* **2008**, *29*, 1538.

LCST was defined as the temperature at which the UV transmittance was altered by 50%. Thermal analysis of the coil-to-globule transition was performed using a differential scanning calorimeter (DSC, Perkin-Elmer Pyris 6). The sample was prepared as a 10 wt % aqueous solution and approximately 15 mg was placed on a sealed aluminum pan. The temperature was increased from 15 to 45 °C at 1 °C/min under a nitrogen flow of 20 mL/min. TEM was performed on a JEOL JEM-1230 instrument with a Gatan Dual Vision CCD camera at 100 kV. Samples were cut into a wedge shape and then embedded in a polyethylene mold using epoxy resin. The specimen was trimmed to a trapezoid shape of approximately 80 nm in thickness, microtomed at rt using a diamond knife on a Leica Ultracut UCT6 system, and collected on a 200-mesh carbon-coated Cu grid for analysis. Tapping-mode scanning force microscopy (Nanoscope 3D, Digital Instruments multimode SPM system, USA; cantilever type SI-DF20, f = 139 kHz, spring constant 16 N m^{-1}) was also used to characterize the surface morphology. Samples were prepared by drop-coating a 0.1 wt % solution onto freshly cleaved wafer substrates and then dried in vacuum at the desired temperature for 24 h before characterization.

Results and Discussion

BBTES Synthesis. The linker with bromide and triethoxysilane functionalities was synthesized by two-step esterification and Michael addition according to Scheme 1A. In the first step, 2-bromo-2-methylpropionyl bromide reacted with HEA to form the bromo-terminated acrylate, as confirmed by the disappearance of the characteristic hydroxyl IR adsorption at 3400 cm^{-1} (Figure 1A). This intermediate further reacted with APTES through Michael addition in the second step. Amine addition to the acrylate afforded a secondary amine in a selective manner and also underwent a second mole addition, controlled by the stoichiometric amount and reaction temperature.[31] For addition of one amine equivalent, the acrylate reacted with APTES at ambient temperature to generate the monobromo-terminated triethoxylsilane, as confirmed by disappearance of the vinyl IR adsorption (−C═C−) at 1637 cm^{-1}. Addition of another mole of acrylate to the secondary amine occurred at a higher temperature (50 °C). The product derived from APTES reaction with two HEA equivalents was very poorly soluble in hexane. On the other hand, the mono-substituted analogue containing one hydroxyl group and APTES was quite soluble in hexane.[32] The ester product with bromide and triethoxylsilane functionalities was then isolated in 72% yield after being washed in hexane.

Tethering the Initiator to NSP. BBTES was allowed to react with NSP in a sol−gel type of reaction in THF. The grafted BBTES (NSP-Br$_2$) was analyzed by ^{29}Si solid-state NMR and FTIR. Pristine NSP exhibited ^{29}Si resonances at −93 and −107 ppm assigned to tetrahedral Q^3 and Q^4. In the layered silicate structures, each Si atom is connected to two or three Si atoms through oxygen bridging, with possible Al or H instead of Si atoms. The resonance denoted as Q^3 (−93 ppm) is attributed to the central Si atom in (−Si−O−)$_2$Si−(O−Al) −OH and Q^4 (−107 ppm) to the central Si in (−Si−O−)$_3$Si(−O−Al).[33] After attachment of the linker, the Q^4/Q^3 intensity ratio for NSP-Br$_2$ increased in comparison to that for pristine

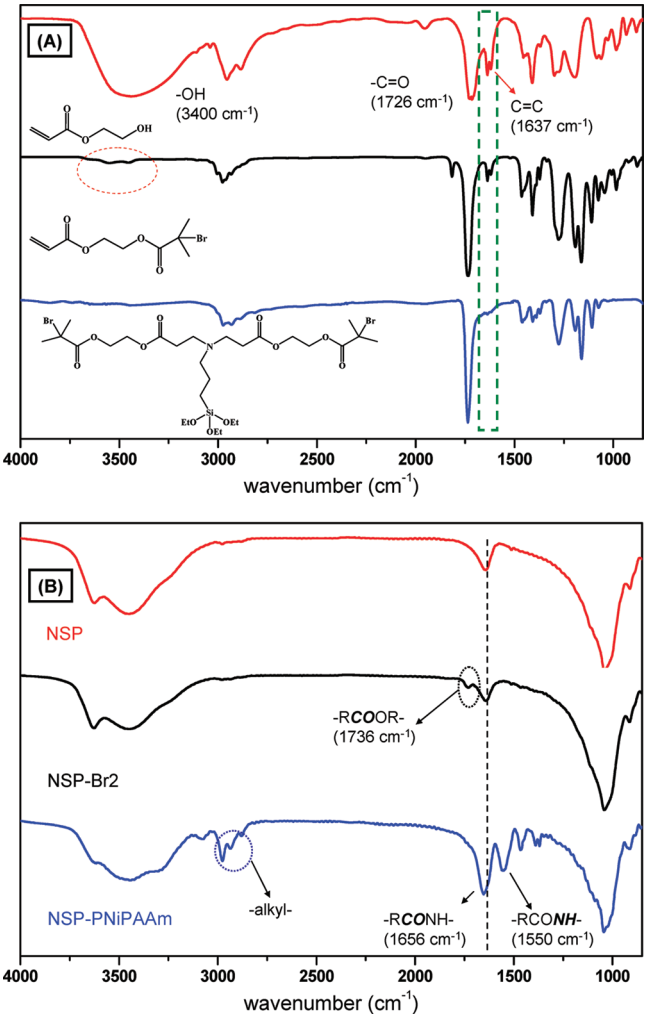

Figure 1. FTIR spectra of (A) HEA, bromo-terminated acrylate, and bis-bromo-triethoxysilane and (B) NSP, NSP-Br$_2$, and NSP-PNiPAAm with amide absorption.

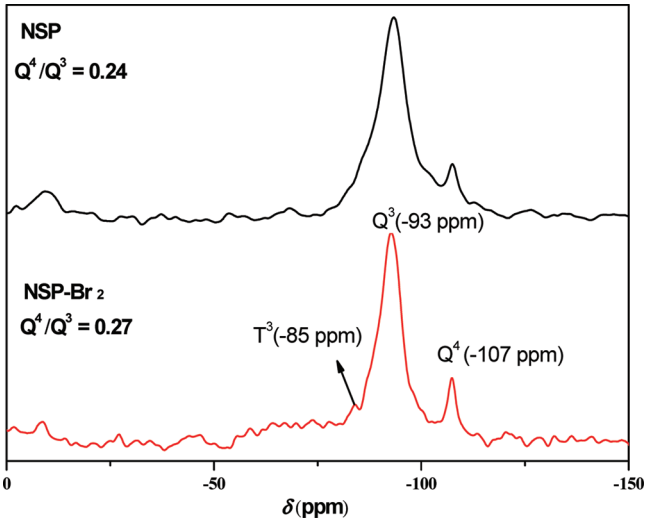

Figure 2. ^{29}Si solid-state NMR spectra of unmodified NSP and modified NSP-Br$_2$.

(31) Wu, D. C.; Liu, Y.; He, C. B. *Macromolecules* **2008**, *41*, 18.
(32) Mori, H.; Miyamura, Y.; Endo, T. *Langmuir* **2007**, *23*, 9014.

Table 1. Preparation and Analyses of NSP-Br_2 from NSP and the Linker

NSP/initiator ratio (w/w)	organic fraction (wt%) calcd[a]	organic fraction (wt%) TGA[b]	amount grafted (mequiv/g)[c]	reactive sites[d]	density (nm^2/site)[e]
5/1	13.9	2.7	0.092	1600	0.50
15/1	5.2	2.3	0.078	1400	0.57
30/1	2.7	1.1	0.037	700	1.14

[a] Organic fraction calculated from initiator amount added. [b] Organic fraction measured between 250 and 600 °C ($W_{250-600}$) during TGA. [c] Amount grafted determined according to eq 1. [d] Approximate number of reactive sites determined according to eq 2. [e] Density calculated as the surface area of the edges (400 nm^2) divided by the number of grafted sites (reactive site/2).

Table 2. Characterization of PNiPAAm on NSP

sample[a]	organic fraction (wt%)[b]	Mn ($\times 10^{-3}$ g/mol)[c]	DP[d]	initiated efficiency (%)[e]	PDI (M_w/M_n)
H1	21	40	350	5.8	1.35
H2	38	84	740	4.9	1.44
H3	50	110	970	4.9	1.50
H4	67	155	1370	4.7	1.21
L1	33	140	1230	3.0	1.40
L2	51	215	1890	2.9	1.28

[a] H, high grafted density of initiator (0.092 mequiv/g); L, low grafted density of initiator (0.078 mequiv/g). [b] Measured by TGA. [c] Measured by GPC using polystyrene standard. [d] Degree of polymerization (DP) determined by the GPC. [e] [(Organic fraction per gram of hybrid/M_w of NiPAAm)/amount grafted]/DP, e.g., $[(0.21/113)/(0.092 \times 10^{-3})]/350 = 0.058$).

NSP (from 0.24 to 0.27) and a small new peak (T^3) appeared at −85 ppm that is attributed to silane compounds covalently grafted to NSP in the form of $(-Si-O-)_3Si-CH_2-$ species (Figure 2). Moreover, NSP-Br_2 displayed IR absorption at 1736 cm^{-1} that is characteristic of the ester group (−R*CO*OR−) in the linker (Figure 1B).

Varying amounts of BBTES were grafted to NSP to control the grafting density. As summarized in Table 1, BBTES/NSP weight ratios of 5:1, 15:1, and 30:1 were used. TGA thermograms of the products exhibit three main decomposition regions.[34] The initial degradation at < 250 °C is attributed to the vaporization of water adsorbed on the clay. The weight loss at > 600 °C is attributed to dehydroxylation of the clay aluminosilicate structure. Only the region between 250 and 600 °C, corresponding to organic decomposition, was considered for quantitative analyses of the grafted linker. Amounts of 2.7, 2.3, and 1.1 wt % correlated to the starting reactions for 5:1, 15:1, and 30:1 NSP/BBTES by weight. Linking of BBTES to reactive sites on the clay is estimated by assuming that the volume of a single NSP is a square of 100 × 100 nm^2 in area for a platelet thickness of 1.0 nm. The density of NSP is 2.86 g/cm^3, similar to that of montmorillonite.[27a] Based on the volume and density, the mass of a single NSP was estimated to be 2.86×10^{-17} g. Accordingly, the number of reactive sites was estimated as 700−1600 per platelet according to the following equation

$$\text{approximately reactive sites} = W_{NSP} \times \left(\frac{W_{250-600}}{1-W_{250-600}}\right) \times \frac{2}{M} \times N_0 \qquad (2)$$

where W_{NSP} is the mass of a single NSP (2.86×10^{-17} g), M is the molecular weight of the linker (588 g/mol), $W_{250-600}$ is the TGA weight loss between 250 and 600 °C corresponding to silane degradation, and N_0 is Avogadro's number. Because natural smectite clay surfaces only have silanol groups (≡Si−OH) at the platelet edges, the BBTES linker could be tethered to the periphery of 1 nm thick NSP over an area of 100 nm × 100 nm (Scheme 1B). Assuming a uniform distribution of sites on the peripheral NSP area (1 nm × 100 nm × 4 = 400 nm^2) for polymer chain growth, the average surface area per grafted site is in the range 0.50−1.14 nm^2.

PNiPAAm Grafting via ATRP. Grafting of NiPAAm polymers was conducted in MeOH/H_2O (7:3 v/v) with a CuCl/PMDETA catalyst at ambient temperature (Scheme 1C). Results are shown in Table 2 for NSP-PNiPAAm of different chain lengths and grafting densities prepared by using various monomer ratios. The grafted PNiPAAm exhibited amide I and II IR bands at 1656 and 1550 cm^{-1}, −NH stretching and two bands corresponding to the deformation of two methyl groups on the isopropyl moiety at 1370 and 1390 cm^{-1} (Figure 1B). A protonic polar cosolvent (MeOH/H_2O) was selected for ATRP so that a hydrogen-bonding solvent could bind to the amide groups of both the monomer and the polymer to reduce their interaction with the catalyst and the propagating chain end.[35] Hence, a narrow molecular weight distribution (1.21−1.50) was obtained for PNiPAAm cleaved in the presence of methanol and catalytic *p*-toluene sulfonic acid.[28b] The molecular weight (Mn × 10^{-3}) of grafted PNiPAAm chains was determined to be 40−215 by GPC. The initiator efficiency calculated from the degree of polymerization (DP) based on TGA and GPC analyses thus represent approximately 5 and 3% for the high and low

(33) Rhee, H. C.; Kim, H. K.; Chang, H.; Lee, J. S. *Chem. Mater.* **2005**, *17*, 1691.
(34) Shanmugharaj, A. M.; Rhee, K. Y.; Ryu, S. H. *J. Colloid Interface Sci.* **2006**, *298*, 854.
(35) Xia, Y.; Yin, X.; Burke, N. A. D.; Stover, H. D. H. *Macromolecules* **2005**, *38*, 5937.

grafting density, respectively (Table 2). Initiator efficiency of 16% has been reported for surface-initiated ATRP of NiPAAm on the surface of silica nanoparticles (~70 nm).[36] The low initiation efficiency in the present study might be a result of steric hindrance caused by the edge effect. In addition, the efficiency decreased with increasing PNiPAAm molecular weight, regardless of the grafting density. Hence, the number of polymer chains grafted to NSP edges was estimated to be 80 and 42 for high and low density, respectively (initiator efficiency × reactive sites, e.g., 1600 × 5% = 80).

Phase Transition of NSP-PNiPAAm. Tests to determine the dispersibility of NSP-PNiPAAm revealed that PNiPAAm was thermoresponsive with LCST of ~32 °C in dilute aqueous solution. This implies that the tethered PNiPAAm undergoes a phase transition from a coil to a globule. Dispersion of NSP-PNiPAAm (0.1 wt %) is temperature dependent because of hydrogen-bonding interactions between PNiPAAm and water. The presence of PNiPAAm renders the NSP dispersible only at temperatures lower than the LCST. This phenomenon of increasing dispersion at lower temperature is described as lower critical aggregation temperature.[37] NSP-PNiPAAm suspensions became optically turbid or rapidly changed to a clear solution in the temperature range 31−34 °C (Figure 3). DSC of NSP-PNiPAAm revealed two second-order transitions in the initial heating process (Figure 4), indicating two different hydration states for PNiPAAm. This heat-induced phase transition was reported elsewhere for PNiPAAm brushes attached to spherical nanoparticles such as gold and SiO_2 during DSC and dynamic laser scattering.[36,38] The phenomenon can be explained by the existence of different density zones for PNiPAAm chains, as shown in Scheme 1C. Two distinct density zones correspond to two different phase transition temperatures (T_{pt}). Presumably, the lower temperature can be defined as the transition temperature for the inner zone, which contains closely packed PNiPAAm segments. Therefore, the inner zone is less hydrated. By contrast, the higher transition temperature can be attributed to loosely packed PNiPAAm in the outer zone. With increasing Mn ($\times 10^{-3}$ g/mol) from 40 to 110 (H1−H3), the phase transition temperature decreased from 29.4 to 26.6 °C for the inner zone and from 36.0 to 27.2 °C for the outer zone (Table 3). Thus, the difference between the two transition temperatures decreased from 6.6 to 0.6 °C. The decrease in both transition temperatures with increasing molecular weight implies that an increase in PNiPAAm concentration results in a decrease in the extent of PNiPAAm hydration. As the chain length increased to 155 Mn ($\times 10^{-3}$ g/mol) or DP = 1370 (H4), the two-stage phase transition merged into a broader first-order transition (Figure 4). This is because the outer zone becomes dominant and masks the effect caused by the inner zone.

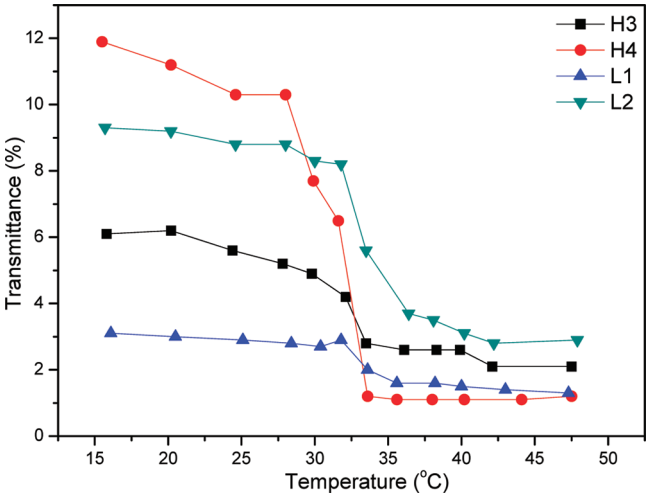

Figure 3. Lower critical aggregation temperature of NSP-PNiPAAm for different chain lengths and grafting densities.

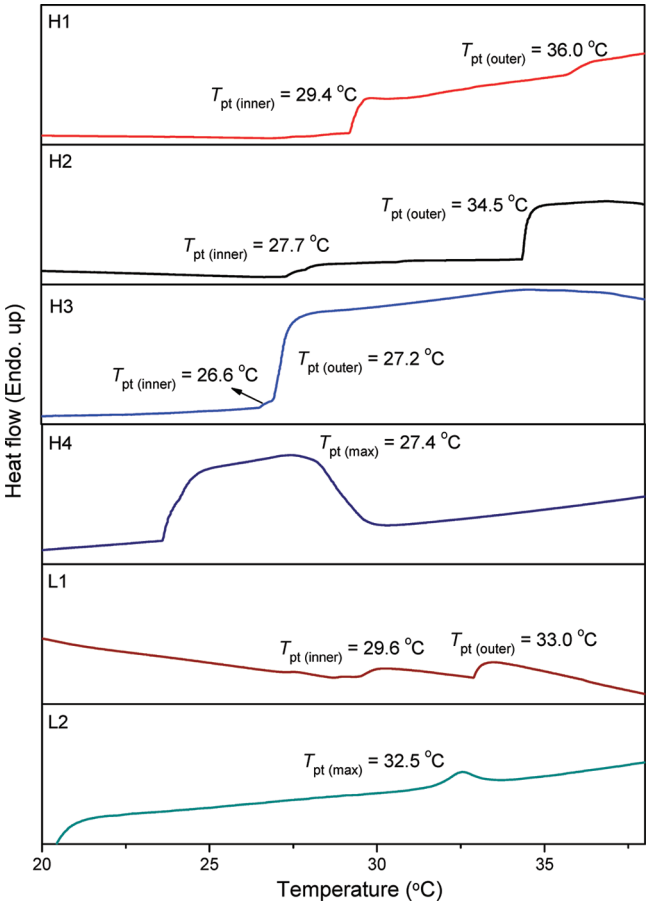

Figure 4. DSC thermograms showing phase transition during the first heating process for NSP-PNiPAAm of different chain lengths and grafting densities.

Table 3 also list values for the change in heat capacity (ΔC_p), which is strongly affected by solvent accessibility to the surface of the polymer chains. In general, polymer segments in the inner zone have more polymer-to-polymer contacts than polymer-to-solvent interactions. However, polymer segments in the outer region have greater

(36) Wu, T.; Zhang, Y.; Wang, X.; Liu, S. *Chem. Mater.* **2008**, *20*, 101.
(37) (a) Lin, J. J.; Wei, J. C.; Juang, T. Y.; Tsai, W. C. *Langmuir* **2007**, *23*, 1995. (b) Lin, J. J.; Wei, J. C.; Tsai, W. C. *J. Phys. Chem. B* **2007**, *111*, 10275.
(38) Shan, J.; Chen, J.; Nuopponen, K.; Tenhu, H. *Langmuir* **2004**, *20*, 4671.

Table 3. Thermodynamic Properties and Phase Transition of NSP-PNiPAAm by DSC

	initial state (first run)[a]				
	T_{pt} (°C)		ΔC_p (kJ/mol °C)		
sample	inner zone	outer zone	inner zone	outer zone	equilibrium state[b] ΔH (kJ/mol)
H1	29.4	36.0	19.1	7.4	0.26
H2	27.7	34.5	15.6	74.8	1.02
H3	26.6	27.2	8.5	133.0	3.74
H4					4.39
L1	29.6	33.0	5.6	8.7	1.16
L2					3.29

[a] Phase transition temperature (T_{pt}) and change in heat capacity (ΔC_p). [b] Change in enthalpy for the phase transition.

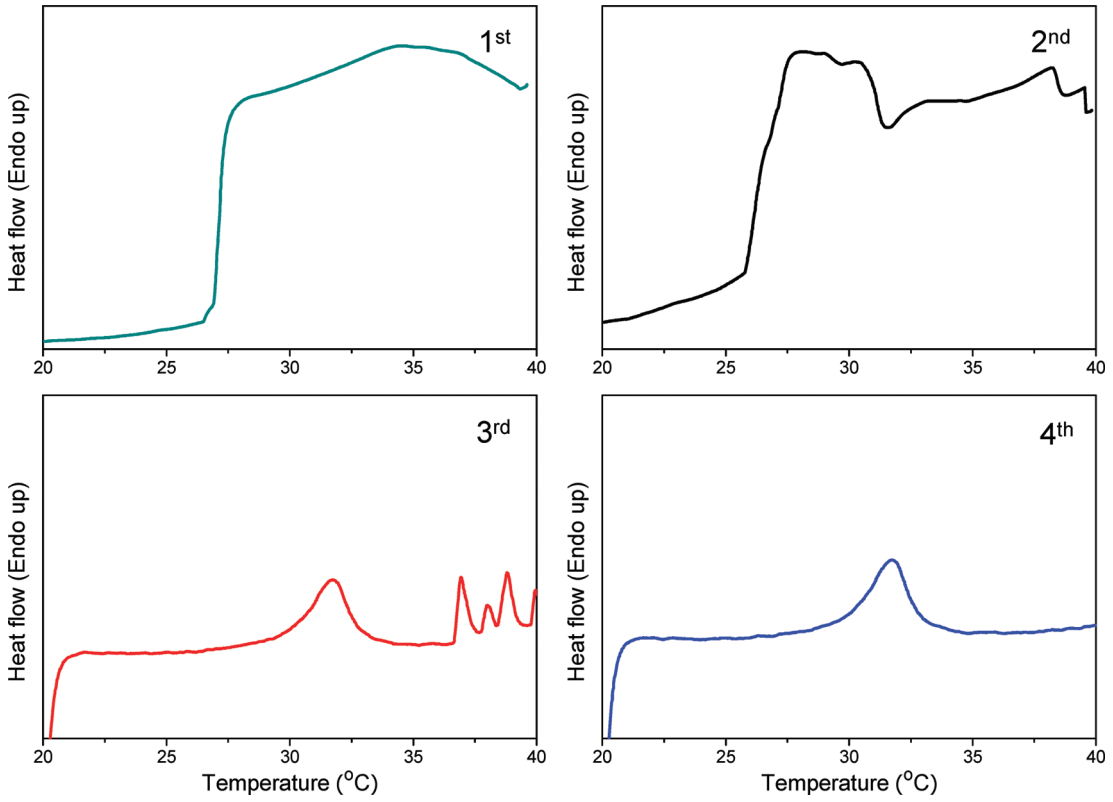

Figure 5. DSC thermograms showing thermodynamic transformation during continuous heating and cooling treatments for the NSP-PNiPAAm hybrid (H3).

accessibility to solvent molecules. For the lengthy polymer chain, the increase in PNiPAAm−H_2O contacts also results in an increase in $\Delta C_{p(inner+outer)}$. In addition, as the chain length increases it becomes more difficult for inner PNiPAAm segments to interact with the solvent and $\Delta C_{p(inner)}$ decreases accordingly. By contrast, an increase in chain length leads to an increase in the thickness of the outer layer and $\Delta C_{p(outer)}$ increases because of greater interaction between PNiPAAm and water. Moreover, for PNiPAAm grafted at lower density (1400 × 3% = 42 polymer chains), sample L1 (DP = 1230) had transition temperatures of 29.6 and 33.0 °C (Table 3). For NSP-PNiPAAm samples L1 and H2 (DP = 740) of similar organic fraction (DP × reactive sites; 1230 × 42 vs 740 × 80), the lower $T_{pt(inner)}$ for H2 than for L1 results from less hydration of the inner zone in the densely packed structure.

NSP-PNiPAAm samples were further examined by DSC in thermodynamic probing (continuously repeated cycles). The two second-order transitions are gradually transformed into a single endothermic first-order transition at ~32 °C (Figure 5). In the first heating process, observation of a second-order transition indicates that hydrogen bonds break between PNiPAAm chains and water molecules. After each cycle, PNiPAAm chains become increasingly densely packed because of inter- and intrachain interactions and finally transform to a condensed packing form. After formation of this condensed NSP-PNiPAAm structure, the first-order endothermic energy transition was reexamined by DSC after storage for 2 days at 5 °C. As shown in Figure 6, the transition behavior remained unchanged. This confirms that the condensed structure with entangled chains and platelets was stable and did not relax back to its original conformation, as shown in Figure 4 (first cycle). In fact, movement of PNiPAAm fixed to NSP is rather restricted. The originally well-dispersed NSP-PNiPAAm formed an aggregate at temperatures above the LCST that remained, even when the temperature was decreased to the LCST.

Figure 7 shows the enthalpy change (ΔH) of the condensed conformation versus the fraction of NiPAAm.

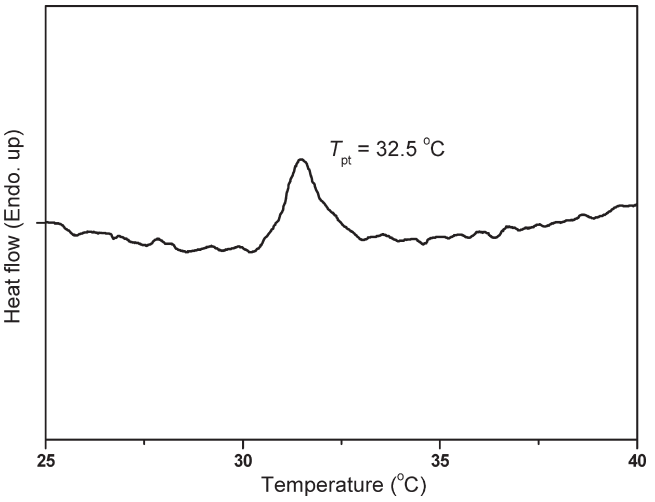

Figure 6. DSC reexamination of the condensed structure of NSP-PNiPAAm (H2) stored for 2 days at 5 °C.

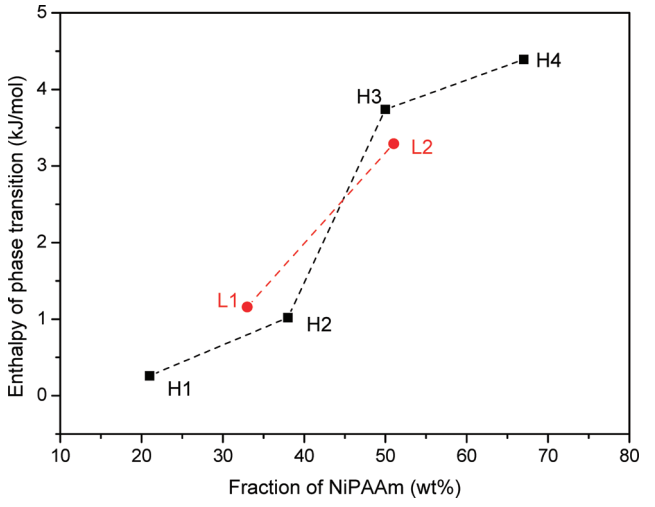

Figure 7. Correlation between the phase transition enthalpy and the polymer fraction in NSP-PNiPAAm.

Samples with similar compositions of NiPAAm (such as H3 and L2, and H2 and L1) have similar ΔH values. The results indicate that the PNiPAAm conformation after several heating and cooling cycles is indeed in the same condensed form and ΔH is only a function of the fraction of NiPAAm, regardless of the chain length or grafting density.

Morphological Transformation of NSP-PNiPAAm. To observe kinetic changes in its conformation, NSP-PNiPAAm was drop-coated on a silicon wafer or glass surface and dried at < 60 °C. The thin film was cross-sectioned and examined by TEM. When formed at temperatures below the LCST, films contained single platelets randomly distributed in the matrix (Figure 8A and B). However, when prepared at temperatures above the LCST, films exhibited an ordered nanostructure that was formed by PNiPAAm segregation. It seems that NSP-PNiPAAm tends to self-assemble through aggregation of the primary structure into secondary PNiPAAm surrounding NSP in separate regions. These NSP and tethered PNiPAAm self-arranged into a 3D spherical network structure on a scale of 100−500 nm. As indicated in Figure 8D and E, the nanostructure consists of an outer shell of clay and an inner core of PNiPAAm regimes. AFM observations confirmed that conformational changes occurred for PNiPAAm chains. At temperatures lower or higher than the LCST, the hybrids formed a smooth interface of coil chains or a globular form at the interface with the NSP edges, as shown in Figure 8C and F, respectively. These observations of a 3D nanodomain network correlate to the thermodynamic transformations during DSC analyses.

Conclusions

A linker with bromide and triethoxysilane functionalities was grafted onto NSP clay surfaces at different grafting densities. Subsequent ATRP afforded NSP-PNiPAAm hybrids. PNiPAAm tethered to NSP hybrids with precise molecular weight control (1.21−1.50 M_w/M_n) is thermoresponsive. It was observed for the first time that

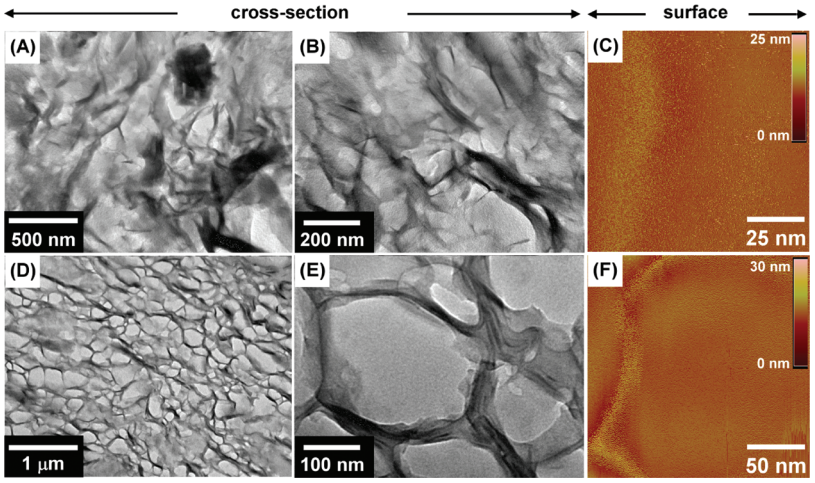

Figure 8. TEM cross-section and AFM surface morphology of self-assembled NSP-PNiPAAm film (H2): (A−C) dried at room temperature or (D−F) dried at 60 °C. (A, B) Random distribution; (C) smoothly coiled PNiPAAm at the interface with NSP edges; (D, E) 3D network structure with nanodomains of 100−500 nm; and (F) globular PNiPAAm at the interface with NSP edges.

NSP-polymer exhibit two second-order phase transition temperatures during DSC heating on interaction with water. PNiPAAm existed in condensed and loose zones when stretching out from the NSP surface. As the chain length increased, these two zones merged and the thermoresponsive LCST property became less distinct. The thermoresponsive phase transformation was translated into self-assembly to form an ordered 3D network structure on drying at temperatures above the LCST. The controllable formation of nanodomain networks of high regularity can be applied to the fabrication of arrays with stimulus-responsive properties.

Acknowledgment. We acknowledge financial support from the Ministry of Economic Affairs and the National Science Council (NSC) of Taiwan.